Participatory Sensing-based Geospatial Localization of Distant Objects Toward Enhanced Disaster Preparedness in Urban Built Environments

Hongjo Kim^a and Youngjib Ham^b

^aAssistant Professor, Department of Civil and Environmental Engineering and Engineering Mechanics, University of Dayton, The United States

^bAssistant Professor, Department of Construction Science, Texas A&M University, The United States

E-mail: hkim01@udayton.edu, yham@tamu.edu (corresponding author)

Abstract

1

2

3

4

5

6

7

8

9

10

11

12

13

14

15

16

17

18

19

20

21

22

23

24

25

Although the benefit of participatory sensing for collecting local data over large areas has long been recognized, it has not been widely used for various applications such as disaster preparation due to a lack of geospatial localization capability with respect to a distant object. In such applications, objects of interest need to be robustly localized and documented for supporting datadriven decision-making in site inspection and resource mobilization. However, participatory sensing is inappropriate to localize a distant object due to the absence of ranging sensors in citizens' mobile devices; thus, the localization accuracy varies to a large extent. To address this issue, this study presents a novel geospatial localization method for distant objects based on participatory sensing. The proposed geospatial localization process consists of multiple computational modules—a geographic coordinate conversion, mean-shift clustering, deep learning-based object detection, magnetic declination adjustment, line of sight equation formulation, and the Moore-Penrose generalized inverse method—to improve the localization accuracy in participatory sensing environments. The experiments were conducted in Houston and College Station in Texas to evaluate the proposed method, and the experimental results demonstrated a reasonable localization accuracy, recording the distance errors of 1.5m to 27.8m when the distance from observers to the objects of interest were 17m to 296m. The proposed method is expected to contribute to rapid data

- 26 collection over large urban areas, thereby facilitating disaster preparedness that needs to identify
- 27 locations of distant objects at risk.
 - Keywords -
- 29 Geospatial Localization; Participatory Sensing; Urban Built Environments

31

32

33

34

35

36

37

38

39

40

41

42

43

44

45

46

47

28

1 Introduction

Participatory sensing has recently emerged to facilitate data collection over large areas with little incremental cost [1,2]. As its name suggests, participatory sensing involves voluntary participations of citizens and community groups in the process of sensing and documenting personal observations. Although the benefit of participatory sensing has long been recognized in various applications including disaster early warning systems [3-5], its utilization is still in its infancy due to practical challenges regarding data reliability and automatic data processing in generating useful information. For example, in the context of disaster preparedness using participatory sensing, it would be necessary to localize vulnerable distant objects from a citizen's mobile device promptly, because their accurate location information helps municipal agencies identify the location and take appropriate actions to prevent potential accidents before extreme weather events. Most municipalities have systems to collect near real-time information of critical infrastructures (e.g., transportation-related infrastructures such as bridges or roads for further inspection), but municipal agencies may not cover local vulnerabilities over large urban areas. The participatory sensing has the potential to be used as a supplementary tool for data collection over large urban areas. Here, it is difficult for local residents to obtain and report the accurate geographic location of distant objects of interest due to the absence of a proper ranging device. Most previous studies have primarily considered the locations of citizens where data were collected due to a lack of a geospatial localization capability for distant objects of interest [6-8]. Such approaches could be valid when accurate location information for distant objects is unnecessary for their applications such as monitoring flooding areas. On the other hand, if an application requires accurate location information for a distant object, a novel localization method needs to be devised to overcome the limitation of citizens' mobile devices—the absence of ranging sensors. Although some studies proposed distant object localization methods using mobile devices [9-14], the dependence on prior information (e.g. BIMs), a heavy computational load for 3D reconstruction, or ranging devices remains as a major obstacle for leveraging participatory sensing. Moreover, the localization accuracy is likely to be exacerbated as the collected data may contain noise by nature and be irrelevant since participatory sensing basically relies on citizens who are not experts [15]. Particularly, three types of noise involved in the collected data—human error, measurement error, and the geospatial proximity of urban objects—would significantly impair the reliability of geospatial localization. These challenges, therefore, militates against the use of participatory sensing for various applications such as the localization of distant objects. To address these challenges, this paper proposes a novel geospatial localization method to identify the geospatial location of distant objects from crowdsourced data collected by citizens' smartphones. On a condition that each crowdsourced data sample contains the followings—an image having an object of interest, a geographic location in a spherical coordinate system, and a compass bearing in the direction toward the object of interest, the proposed method can localize distant objects building upon sequential computational modules. The premise of such data availability is founded on the fact that most smartphones can be easily used to collect their

48

49

50

51

52

53

54

55

56

57

58

59

60

61

62

63

64

65

66

67

68

69

geographic locations, compass bearings, and images, as conducted in many previous studies regarding participatory sensing [6,12,16]. Each module in the proposed method is designed to address the data reliability issue in utilizing crowdsourced data for geospatial localization. This study contributes to a methodological aspect and understanding for geospatial localization in participatory sensing by presenting how distant objects in urban areas can be robustly localized from multiple observations through the novel localization process. In experiments, the proposed method demonstrates the capability of each module to improve the reliability of geospatial localization using crowdsourced data, addressing three types of noise such as human error, measurement error, and the geospatial proximity of urban objects. This study is expected to promote the utilization of crowdsourced data to improve collective readiness in urban areas with respect to extreme weather events, as shown in Fig. 1. The following section introduces previous studies related to participatory sensing for disaster management and geospatial localization methods, and then the detailed computational process for localization is discussed.

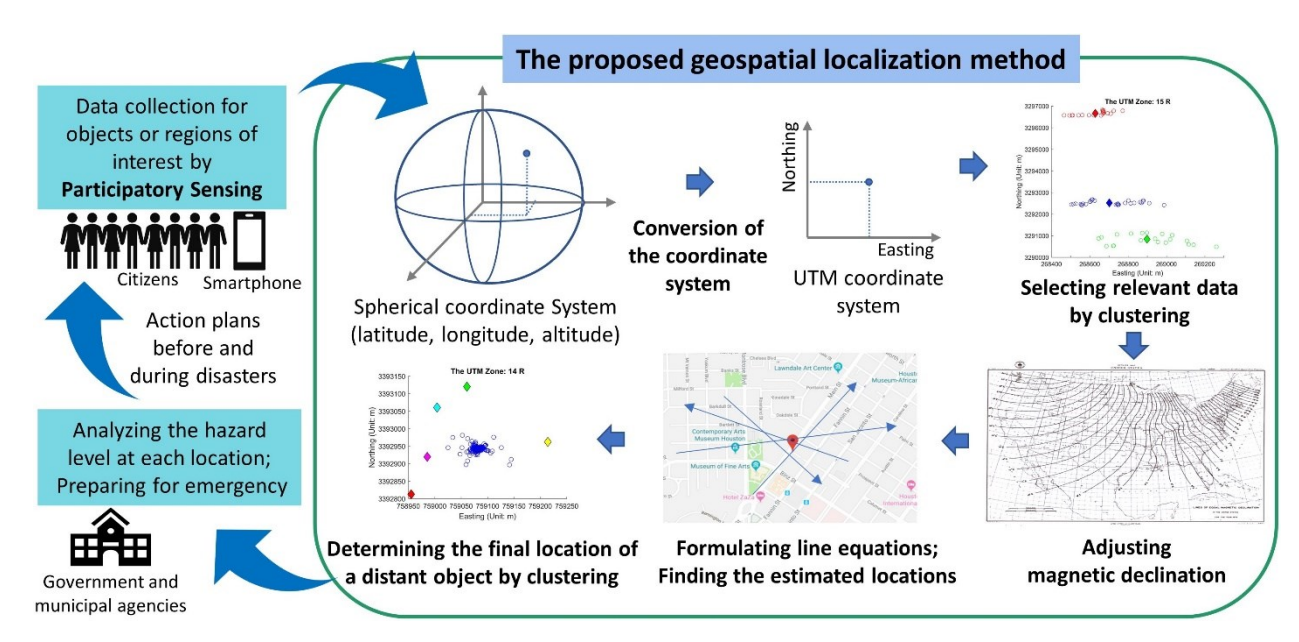


Fig. 1 Conceptual diagram of participatory sensing for improving disaster preparedness

2 Background

86

87

88

89

90

91

92

93

94

95

96

97

98

99

100

101

102

103

104

105

106

107

108

2.1 Data utilization for management applications in urban areas

Over the past decades, many studies have investigated data-driven methods for various applications in urban built environments such as disaster management and infrastructure asset management. For example, structural damage monitoring methods regarding disaster impact analysis have been widely studied, using imaging devices such as LiDAR (Light Detection and Ranging) [17,18], optical cameras [19,20] and embedded sensors [21]. These methods provided valuable insights for how to analyze the damage and response of structures from image or signal data during and after disaster situations. In emergency response and recovery phases, a mobile adhoc network, radio frequency identification (RFID), a geographic information system (GIS), and a mobile workstation chariot were utilized for facilitating communication between first responders (e.g. structural engineers and fire fighters), building damage assessment, and resource allocation [22-25]. Depending on the data type, available information for an object of interest varies. The field data types can be largely divided into text, signal, and imagery. Text is generally a secondary data representing human's judgment in linguistic expressions with regards to an object of interest. Signal data can represent the physical quantity with respect to stress, pressure, strain, temperature, voltage, current, or magnetic force; thus, such data can be transformed into useful information including structural performance and physical condition for assessing infrastructure vulnerability [21] and detecting abnormalities in facilities [26] under disaster events. Signal data has been used to provide location information for safe excavations of underground utility pipelines [27] or planning evacuation of people trapped inside buildings under disaster situations [28]. On the other hand, image data can represent the visual appearance of the real world that represents the shapes

and textures of objects; thus, a person can understand a physical characteristic of objects or a scene context. Based on image data, the condition and serviceability of buildings and infrastructures have been investigated for post-disaster damage assessment [29] or maintenance and repair of infrastructures [30]. Although image data is a two-dimensional representation of the real-world, it can provide three-dimensional information by reconstructing depth information. For the reconstruction of depth information, the structure-from-motion algorithm has been widely used; the reconstructed 3D information has provided valuable information for managing transportation infrastructure assets [31], recovering the structural drawing images of damaged buildings [19], and assessing residential building damages [20]. However, the reconstruction accuracy is relatively lower than the accuracy of 3D information collected by 3D imaging devices such as LiDAR. The 3D imaging devices can collect 3D images (or point clouds) through their active sensor which emits radiation to measure depth information at a point of an object or scene. Based on accurate 3D information, various research projects and applications have been established in the Architecture, Engineering, Construction, and Facility Management (AEC/FM) industry [32], such as damage assessment for building properties [18] and reinforced concrete frames [33]. Building on various types of data, a few studies have utilized simulation methods to analyze emergency response of citizens during natural disasters to establish proactive action plans [34-37]. Despite their benefits, there has been a dearth of study dedicated to developing an effective data collection method having scalability over large areas. Although sensor networks and imaging devices can provide information to be effectively scaled up, it is not trivial to install sensor networks in existing infrastructures and collect image data with limited human resources; collected data should be processed with computationally expensive algorithms to detect target objects and analyze their vulnerabilities. The lack of scalable data collection methods motivates this study to investigate an

109

110

111

112

113

114

115

116

117

118

119

120

121

122

123

124

125

126

127

128

129

130

alternative method that can efficiently scale up the data collection capability over large areas with the help of people and existing sensors.

134

135

136

137

138

139

140

141

142

143

144

145

146

147

148

149

150

151

152

153

154

132

133

2.2 Participatory sensing

Participatory sensing has been utilized to identify local information from citizens for various applications such as disaster risk reduction [38,39]. Stemming from citizen science projects, participatory sensing generally consists of five steps such as (1) recruiting participants, (2) educating participants how to collect and analyze local data, (3) collecting local data, (4) analyzing the collected local data, and (5) reporting the local data using participants' mobile devices. It has attracted considerable research interests in academia as an alternative data collection tool, because of its scalability over large areas based on citizens' mobile devices [1,2,39]. In the general process of participatory sensing, citizens voluntarily and intentionally upload local information through social media or smartphone application. Leveraging social media as a new data storage and collection platform, previous studies have presented a way of collecting and utilizing crowdsourced data such as images and texts regarding natural disasters for emergency management, through transforming crowdsourced data into key information to enhance situational awareness during natural disasters [6,40,41]. Particularly, crowdsourced data has shown its usefulness for monitoring flood damage in urban areas [39,42-44]. Providing such flood damage maps has the advantage of understanding the flood damages over large areas at once, which facilitates establishing a prompt recovery plan. A few studies proposed a way to improve disaster response by monitoring local situations during heavy rainfalls through social media data for warning local residents at risk [7,8]. Crowdsourced data has been mostly collected from social media, composed of several data types such as images, texts, and geographic locations [6,7,40-44]. In some cases, image data was collected by Closed Circuit Television (CCTV) [8] and GIS data was collected through volunteered geographic information mapping platforms such as OpenStreetMap (OSM) [39].

However, there have been little discussion about improving disaster preparedness based on participatory sensing, though its potential of reducing disaster-induced damage has long been recognized [3-5]. To reduce the impact of natural disasters, it is critical for citizens to be well-prepared based on the local information about potential hazardous objects and areas. Such information enables citizens to be informed about where not to go and where not to stay for their safety during extreme weather events and allows governmental agencies to mobilize their limited resources at vulnerable areas to prevent losses and accidents from occurring. Thus, it is necessary to identify vulnerable objects in local areas prior to a natural disaster arrives. For example, windstorms—the second most frequent natural hazards—could lead to crane collapse in urban construction sites which often causes secondary damage to neighboring critical infrastructure such as roads or power grids and serious injury and death to nearby people [45]. Here, participatory sensing has significant potential for rapidly investigating such local vulnerabilities over large urban areas with little incremental cost. To this end, participatory sensing should be equipped with the geospatial localization capability, thereby enabling to localize target objects that need to be reported at the right time.

2.3 Previous studies of geospatial localization

Herein, the definition of geospatial localization refers to the process of localizing an object or area in world coordinate systems such as the Global Positioning system and the Universal

Transverse Mercator system. Geospatial localization methods for a distant object using smartphones have been studied in the last decade for various purposes such as indoor/outdoor navigations and models/databases update [46]; most previous studies have utilized images to estimate the geospatial location of a distant object in urban areas, while using a users' geographic location as a reference location. Previous geospatial localization methods can be categorized as indirect methods and direct methods [46]. In either category, the localization methods involve reconstructing or finding camera pose information since it is crucial to infer the geometric relationship between 2D images and the 3D real world. Following this fundamental principle, localization methods have also been studied in the civil engineering domain for construction site or built environment management applications. Balali et al. [31] presented traffic sign recognition and localization method using 3D reconstruction and machine learning techniques. Ham and Yoon [9] proposed a distant object localization method that employs user's motion information and image contents, by integrating different types of information collected by embedded sensors in smartphones such as an accelerometer, magnetic field, gyroscope, and camera sensors. Ha et al. [14] utilized a building information model (BIM) and a convolutional neural network to localize a scene shown in a mobile head-mounted display. Kim et al. [10] developed a hazard avoidance system using a wearable device which displays the direction of a closest construction vehicle nearby a user and its hazard level, by localizing construction entities through stationary cameras with a predetermined monitoring environment. Although these studies have reported promising localization accuracies, their method requires additional information such as BIM or dedicated cameras for monitoring, which are not generally available for localization purposes in most urban areas. Otherwise, 3D reconstruction is inevitable to infer a 3D real-world geometry of 2D scenes for localization. However, 3D reconstruction algorithms such as structure-from-motion are

177

178

179

180

181

182

183

184

185

186

187

188

189

190

191

192

193

194

195

196

197

198

computationally expensive to timely localize multiple objects in large areas. Recently, a few studies proposed geospatial localization methods for urban environments using photographers' locations, shooting angles and images [11-13], but their methods showed unstable localization accuracies (discussed in more detail in Section 5). To improve and stabilize the geospatial localization accuracy, this study presents a novel way to localize distant objects using multiple observations collected by citizens' smartphones, described in the following section.

3 Participatory sensing-based geospatial localization

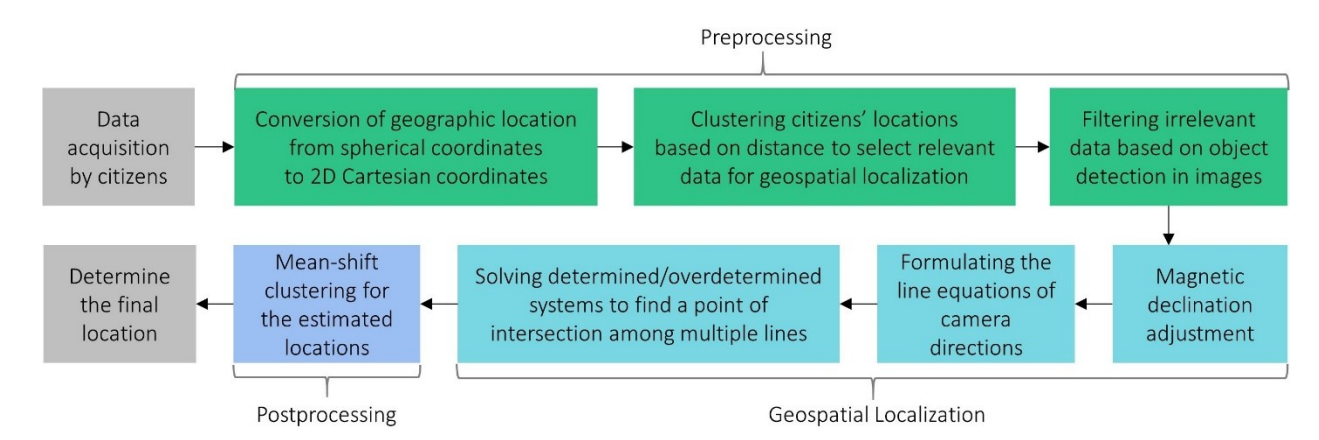


Fig. 2. Overview of the proposed geospatial localization method.

The proposed geospatial localization method, as shown in Fig. 2, is designed to localize static distant objects using crowdsourced data in which each data sample includes an image having an object of interest, a geographic location in a spherical coordinate system, and a compass bearing in the direction toward the object of interest. Fig. 3 illustrates the data acquisition process —image acquisition and sensor data documentation: Participants take a picture of a distant object, and then record an embedded sensor data (geographic location and compass bearing) through a smartphone application while pointing the smartphone toward the distant object. Any smartphone application

can be used if it can be used to collect the three types of data—a geographic location, a compass bearing, and an image. Collected images are used for filtering irrelevant data in the preprocessing step; geographic locations and compass bearings are used to cluster adjacent data samples and to formulate line equations that represent directions toward a distant object; the intersection points among the line questions determines the estimated locations of a distant object; the final location of a distant object is determined by finding the cluster center of a cluster having the majority of the estimated locations.

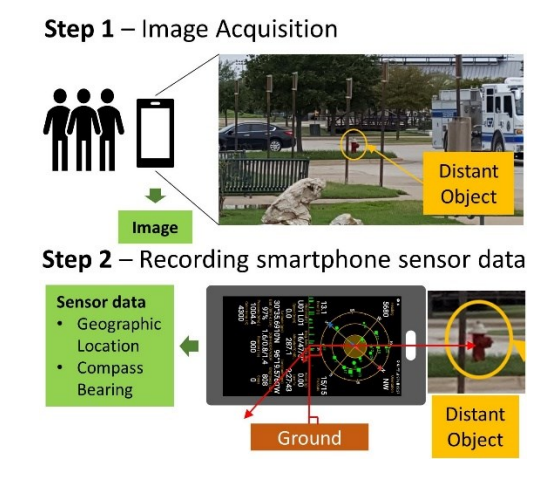


Fig. 3. Data acquisition process with a smartphone.

The three types of data can be easily collected by multimodal sensors embedded in consumer-level smartphones. However, in participatory sensing, the reliability of crowdsourced dataset is typically inconsistent since it is likely to involve noisy data, which impairs the accuracy of the analytic results [47]. For geospatial localization of distant objects, three types of noise would be involved in crowdsourced dataset such as (1) human error, (2) measurement error, and (3) the geospatial proximity of urban objects: Human error occurs when a citizen takes a photograph of wrong objects which are not of interest and thus records an unnecessary compass bearing. It is also human error that citizens mishandle their smartphones when measuring a geographic location or a

compass bearing. Measurement error signifies the difference between a measured value and its true value; this error likely occurs when a geographic location and a compass bearing are measured by a citizen's mobile device, due to the inaccuracy and imprecision of mobile sensors embedded in consumer-level smartphones. The geospatial proximity of urban objects represents a case when different urban objects in a close distance are simultaneously reported. In this case, irrelevant data that is not indicating an object of interest might be included in the localization process, therefore, resulting in inaccurate localization results.

3.1 Preprocessing the crowdsourced data: conversion, clustering, and filtering the

crowdsourced data

The preprocessing part consists of three modules for two objectives: the conversion of a geographic location from spherical coordinates to two-dimensional Cartesian coordinates and the selection of data relevant to a specific distant target object from entire crowdsourced dataset. At the first preprocessing module, an initial geographic location data in spherical coordinates (Latitude/Longitude in degrees-minutes-seconds and Altitude in meters) is converted into the Universal Transverse Mercator (UTM) system, which represents the location in two-dimensional Cartesian coordinates (Easting/Northing in meters) within a UTM zone. By doing so, the formulation of a line equation toward a distant object can be simplified in the two-dimensional space, using a single geographic location with a compass bearing. In this way, the localization of a distant object can be done by finding the point of intersection of multiple line equations in the UTM system (discussed in Section 3.2).

The purpose of the second preprocessing module is to select relevant data for a specific urban object by the mean-shift clustering with respect to the citizens' location, based on the assumption

that a geo-cluster of crowdsourced data corresponds to a single object of interest in a large urban area. To this end, the mean-shift clustering algorithm Yizong [48] is employed in this module. Among various clustering algorithms, the mean-shift clustering was selected due to the simplicity in optimizing its parameters. Moreover, the mean-shift clustering does not require to specify the number of clusters before clustering. It accurately separates data points into a random number of clusters based on the spatial distribution of data points. This characteristic is important in the context of participatory sensing since the number of distant objects is generally unknown in advance. Given a set of location data points, the mean-shift algorithm finds a local mode—the maximum of a kernel density function—of data points in a circular window; if the mode is found, the window is centered on the mode, and this process iterates until a mode converges. Location data points traversed by the window towards a same converged mode constitute a cluster; data points in a cluster are used to localize a specific distant object. Fig. 4 shows an example of the mean-shift clustering for location data points of citizens in the UTM system.

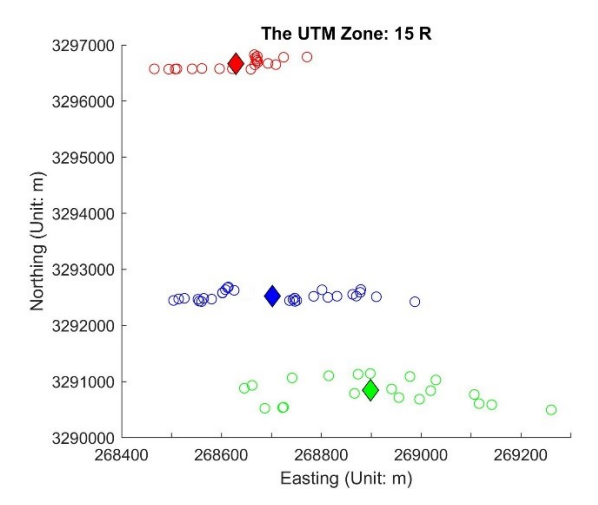


Fig. 4. Examples of the mean-shift clustering results (Circles: observers' locations,

Diamonds: cluster centers).

278

279

280

281

282

283

284

285

286

287

288

289

290

291

292

293

294

295

296

297

Although crowdsourced data can be clustered by distance, a cluster may have some data samples irrelevant to an object of interest. To filter out such irrelevant data samples, the third preprocessing module employs an object detection model for image analysis. Among various object detection models, the region-based fully convolutional network (R-FCN) [49] is leveraged, which is a type of deep neural networks to detect objects of interest in images. Deep neural networks have received considerable attention in recent years, because of its high performance in various tasks such as computer vision, speech recognition, and natural language processing [50]. Generally, deep neural networks extract data representations from input data in successive layers and use the extracted data representations to label a category for the input data. Specifically, R-FCN, which is dedicated to object detection in images, consists of three major components including a 50-layer residual network, a regional proposal network, and position-sensitive pooling layers; through these components, R-FCN searches a target object at every pixel location based on the scores of extracted visual features in multiple grids. However, its accuracy is not easily guaranteed unless a large amount of training data is provided for each target class or a special training process is applied. Because training image data for target classes are not sufficiently available, this study adopts transfer learning in the training process to secure the high detection accuracy of R-FCN. Under the transfer learning scheme, R-FCN model pretrained with a large amount of data in a different domain is retrained with training data regarding target object classes in this study. Based on the detection results in a cluster, irrelevant data are removed to enhance the geospatial localization accuracy of the proposed method.

3.2 Geospatial Localization

299

300

301

302

303

304

305

306

307

308

309

310

311

312

313

314

315

316

317

318

319

320

321

The principle of the proposed geospatial localization is to find the point of intersection of multiple line equations that direct to a distant object of interest; the point is regarded as the distant object's location. To do so, geographic locations of smartphones and compass bearings are used to cluster adjacent data samples; and data samples in a cluster are then used to formulate line equations that represent the directions toward a distant object. However, the value of a compass bearing should be adjusted considering magnetic declination before line formulation since the initial compass bearings correspond to the direction toward the magnetic north of the Earth, rather than the true north. Magnetic declination (also called magnetic variation) refers to the angle difference between the true north and the magnetic north, which varies in extent at different locations by the Earth's magnetic field. Since the magnetic sensor in smartphones outputs the value of a compass bearing based on the magnetic north, the deviation associated with the recorded compass bearings would lead to the inaccurate localization results for a distant object. To represent the accurate angle toward the true north, the compass bearings are adjusted by magnetic declination at each geographic location, referring to the International Geomagnetic Reference Field Model [51]. Based on the adjusted compass bearing along with geographic location of smartphone, a line equation toward a distant object of interest is formulated. In principle, the estimated locations of a distant object can be obtained by solving multiple line equations, even if the number of line equations is greater than the number of unknowns (x, y)—Easting and Northing. When the number of line equations is 2, a determined system of the line equations is solved by using an inverse matrix of line equations. Otherwise, when the number of line questions is greater than 2, an over-determined system of the line equations is solved by using the Moore-Penrose generalized inverse method [52] to obtain a unique solution for a distant object's location. The detailed process

of the geospatial localization is explained in Appendix.

323

324

325

326

327

328

329

330

331

332

333

334

335

336

337

338

339

340

341

342

343

344

322

3.3 Postprocessing the estimated locations

The proposed method can produce multiple estimated locations for a single urban object by selecting different combinations of data samples or using different numbers of lines for localization. Here, the localization accuracy of each estimated location is likely to vary to a large extent due to data uncertainty and inconsistency from multimodal sensors embedded in mobile devices. To stabilize the localization accuracy, a statistical inference method is employed to determine the location of a distant object building upon multiple estimations. The underlying assumption is that when multiple estimated locations are generated for a distant object, their geographic distribution most likely converge on the ground truth location of the distant object since each estimated location is an approximation of the ground truth location. In this context, the cluster center of the estimated locations is likely closer to the ground truth location than most estimated locations. To localize a distant object based on this assumption, the statistical inference first produces many estimated locations using the proposed localization method described in Section 3.2. Since multiple observations can be reported for a single distant object, the maximum number of possible estimated locations is calculated by counting the number of k-combinations out of n data samples, $\sum_{k} {n \choose k}$, where k = [2, 3, ..., n] is the number of line equations used in geospatial localization and n is the number of data samples in a selected cluster. For example, when n is 10, 20, and 30, the maximum number of combinations of estimated locations by taking k line equations is 1013, 1,048,555, and 1,073,741,793, respectively. For computational efficiency, a set of k can be differently determined considering the number of data samples—n. After generating multiple estimated locations, the mean-shift clustering algorithm divides the estimated locations into several clusters. Here, the final location of a distant object is determined as the center of a cluster having the largest number of the estimated locations, which helps eliminate outlier locations estimated based on erroneous data.

4 Experiments

In our experiments, as a proof concept, before the data collection, participants were instructed regarding the data collection process (i.e., what to document, how to take photos involving target objects, how to record the direction information using a dedicated smartphone application while pointing the smartphone toward the objects). In our experiments, it was observed that it takes around ~10 seconds per instance. Although reporting the direction information after taking a photo would be burden as it requires additional effort, but it was observed that such activity did not lead to significant discomfort or resistance to participants during our experiments.

The proposed geospatial localization method was tested on a computer with the configuration of the Intel i7-6700 CPU and the GTX1080 8GB GPU in the Ubuntu 16.04 operating system. Two classes of objects—a fire hydrant and a tower crane in urban areas—were selected as distant objects of interest to evaluate the proposed method. A tower crane was selected since it has been considered as one of the most vulnerable objects in dense urban areas with respect to severe wind-related events. Moreover, as one of critical infrastructure distributed in urban areas, fire hydrants were also selected in the case studies to evaluate the effectiveness of the proposed mean-shift clustering module. Datasets used in the experiments are shown in Tables 1-5. To collect data regarding the distant objects using smartphones, participants first captured images containing the distant objects of interest and then measured compass bearings by pointing their smartphone at the

objects. Following this process, the data samples of two fire hydrants and a tower crane were collected using a cell phone (Samsung Galaxy Note5) in College Station and Houston in Texas, respectively. Fig. 5 shows the ground truth locations of the target urban objects in the two different regions. To evaluate the localization accuracy, the difference between the ground truth location of the distant objects and a final estimated location was measured; the object detection performance in the preprocessing step was presented in form of mean average precision (mAP), which is an evaluation index of many visual task challenges such as the Common Objects in Context (COCO) challenge and the ImageNet Large Scale Visual Recognition (ILSVRC) challenge. The magnetic declinations of +2°58' in College Station and +2°23' in Houston were used for adjusting the compass bearings of the collected data in the entire experiments.



Fig. 5. The ground truth locations in the UTM coordinate system of two fire hydrants in College Station, TX and a tower crane in Houston, TX (FH: fire hydrant, CR: tower crane). The enlarged regions display the data collection areas and the green dots represents the data sample locations.

Table 1. Data samples for fire hydrant #1 in College Station, Texas.

Target	Compass Bearing (°)	Latitude (°)	Longitude (°)
FH1-1	146.7	30.59485	96.3279
FH1-2	172.4625	30.59478	96.3277833
FH1-3	194.2875	30.59495	96.3278333
FH1-4	208.74375	30.59493	96.3277833
FH1-5	226.29375	30.5949	96.3276833
FH1-6	221.90625	30.59497	96.3275833
FH1-7	210.6	30.59503	96.3276333
FH1-8	197.94375	30.59515	96.32765
FH1-9	182.98125	30.5951	96.3277333
FH1-10	171.28125	30.5952	96.3278333
FH1-11	155.7	30.59512	96.3279833
FH1-12	145.29375	30.59513	96.3281
FH1-13	150.075	30.59505	96.3280167
FH1-14	19.29375	30.5946	96.3279167

FH1-15	5.85	30.59445	96.3278667
FH1-16	24.75	30.59438	96.3280167
FH1-17	71.2125	30.5947	96.32805
FH1-18	115.93125	30.59485	96.32795

Table 2. Data samples for fire hydrant #2 in College Station, Texas.

Target	Compass Bearing (°)	Latitude (°)	Longitude (°)
FH2-1	212.56875	30.64152	96.2963333
FH2-2	213.75	30.64153	96.29625
FH2-3	223.81875	30.6415	96.2962333
FH2-4	235.4625	30.64147	96.2960167
FH2-5	242.71875	30.64142	96.29595
FH2-6	255.43125	30.64125	96.2959667
FH2-7	245.8125	30.6413	96.2961
FH2-8	261.5625	30.64117	96.29595
FH2-9	269.8875	30.6411	96.2959667
FH2-10	279.61875	30.64095	96.296
FH2-11	295.03125	30.64078	96.2960167
FH2-12	306.05625	30.6407	96.29615
FH2-13	328.78125	30.64057	96.2964167
FH2-14	344.75625	30.6406	96.2966167
FH2-15	354.9375	30.64062	96.2967167
FH2-16	15.69375	30.64062	96.2969667
FH2-17	45.16875	30.64065	96.2971833
FH2-18	57.99375	30.64083	96.2972
FH2-19	79.36875	30.64097	96.2972167
FH2-20	96.58125	30.64112	96.2972167
FH2-21	106.59375	30.64125	96.2972833
FH2-22	119.53125	30.64135	96.2971167
FH2-23	133.425	30.6415	96.2970667
FH2-24	146.8125	30.6415	96.297
FH2-25	174.09375	30.64155	96.2967667

Table 3. Noisy data samples for fire hydrant #2 in College Station, Texas.

	Target	Compass Bearing (°)	Latitude (°)	Longitude (°)
_	Noisy FH2-1	155.30625	30.6411	96.2972167
	Noisy FH2-2	287.94375	30.6410667	96.2972167
	Noisy FH2-3	8.325	30.6410833	96.2971833
	Noisy FH2-4	52.70625	30.6410833	96.2971833

Noisy FH2-5	222.24375	30.6410833	96.2971833
Noisy FH2-6	43.70625	30.6412667	96.2972
Noisy FH2-7	5.56875	30.6412	96.29675
Noisy FH2-8	84.31875	30.6412667	96.2966667
Noisy FH2-9	325.74375	30.64125	96.2967167
Noisy FH2-10	268.81875	30.64135	96.2970667
Noisy FH2-11	319.6125	30.6415333	96.29655
Noisy FH2-12	340.0875	30.6415333	96.2966
Noisy FH2-13	6.24375	30.6415167	96.2966
Noisy FH2-14	32.5125	30.6415167	96.2966167
Noisy FH2-15	48.31875	30.6415167	96.2966167
Noisy FH2-16	74.64375	30.6415333	96.2966167
Noisy FH2-17	112.21875	30.6415333	96.2966333
Noisy FH2-18	135.9	30.6415333	96.2966333
Noisy FH2-19	145.125	30.64155	96.2966167
Noisy FH2-20	184.95	30.6413833	96.2968667
Noisy FH2-21	240.975	30.6413	96.29705

Table 4. Data samples for a tower crane in Houston, Texas.

	T		
Target	Compass Bearing (°)	Latitude (°)	Longitude (°)
CR1-1	137	29.77783	95.39295
CR1-2	177	29.77945	95.3928833
CR1-3	160	29.77923	95.39285
CR1-4	162	29.77918	95.3928667
CR1-5	165	29.77895	95.3928333
CR1-6	176	29.77877	95.3926167
CR1-7	191	29.77858	95.39245
CR1-8	164	29.77855	95.3928833
CR1-9	167	29.77972	95.3929
CR1-10	163	29.77992	95.3928667
CR1-11	161	29.78017	95.3929333
CR1-12	177	29.77977	95.3923167
CR1-13	188	29.77982	95.3918333
CR1-14	112	29.77785	95.39495
CR1-15	100	29.7778	95.39465
CR1-16	106	29.77783	95.3945167
CR1-17	104	29.77787	95.3944833
CR1-18	101	29.77787	95.3941667
CR1-19	101	29.77793	95.3939667
CR1-20	107	29.7779	95.3936
CR1-21	102	29.7779	95.3933333

Table 5. Ground truth coordinates of urban objects in the UTM system

Object	Latitude (°)	Longitude (°)
FH1	30.594726	96.3279041
FH2	30.641061	96.2967157
CR1	29.777722	95.3926044

394

395

396

397

398

399

400

401

402

403

404

405

406

407

408

409

410

411

412

392

The eighteen data samples of the first fire hydrant, as shown in Table 1 and the right column of Fig. 6, were collected by smartphones at a distance ranging from 17m to 54m (average distance: ~34m); for the second fire hydrant, a dataset of the twenty five data samples in Table 2 and the left column of Fig. 6 were collected at a distance ranging from 47m to 84m (average distance: ~62m). In addition, 21 noisy data samples having incorrect compass bearings were collected nearby the fire hydrant #2, to evaluate the localization performance of the proposed method in challenging conditions for participatory sensing. At the first preprocessing module, the spherical coordinates of the data samples were converted to the UTM coordinates. In the case study, the search window size during the mean-shift clustering was empirically determined to be 400m in diameter. It was observed that the mean-shift clustering module for selecting relevant data samples successfully separate the data samples into two clusters, each of which related to a different object, as shown in Fig. 7. To filter irrelevant data samples at the preprocessing module, the object detection model was trained with the setting of 53 training samples for fire hydrants, 230 training samples for tower cranes, and 10,000 training iterations; the number of test samples was 49 for fire hydrants and 57 for tower cranes. During the experiments, each image size was changed for enhancing computational efficiency such that the sizes of the training and test images were adjusted to have their shortest image side of 800 and 1,080, respectively, while keeping the aspect ratio considering the GPU memory limit (e.g., an image of 3000×2000 is adjusted to 1200×800). To detect each object class having a relatively different size in images, the range of anchor box

sizes (i.e., the size of a candidate region used to find a target object in a region proposal network [53]) was changed from 128², 256², and 512² pixels to 8², 16², 32², 64², 128², and 256² pixels. With this experimental setting, mAPs of 95.62% and 74.67% were reported by the object detection model for fire hydrants and tower cranes, respectively. Based on the trained detection model, the presence of target objects in images were identified, and then only relevant data samples were fed into the geospatial localization. To estimate the location of each object, the line equations of the remaining data samples were formulated; among the line equations, two lines were randomly selected 300 times to produce 300 estimated locations by solving equation (3) in Section 3.2. At the postprocessing step, the search window size of the mean-shift clustering was empirically set to 40m in diameter in the case study. The center of a cluster with the largest number of the estimated locations was determined as the final location and then the distance error was measured, by calculating the distance between the final location and the ground truth location, as shown in Fig. 8. The location of a tower crane in urban construction sites in Houston, TX, was also estimated to evaluate the performance of the proposed method in a case when observer-to-object distances were relatively longer. For the tower crane, 21 data samples were collected at a distance ranging from 68m to 296m (average distance: ~186m). Table 6 shows the experimental results of the proposed geospatial localization method in the case study, which were obtained by averaging 300 localization results. The distributions of the distance error for each object were represented in form of histograms, as shown in Fig. 9. To investigate the impacts of noisy data, the number of line equations, and the number of data samples, additional experiments were conducted. Two lines equations were selected to generate 300 estimated locations in all experiments, except for the experiment regarding the number of data samples. All reported errors were calculated by averaging 300 localization results, and the average computation time per each localization was 0.106s.

413

414

415

416

417

418

419

420

421

422

423

424

425

426

427

428

429

430

431

432

433

434



Fig. 6. Examples of the R-FCN-based object detection results.

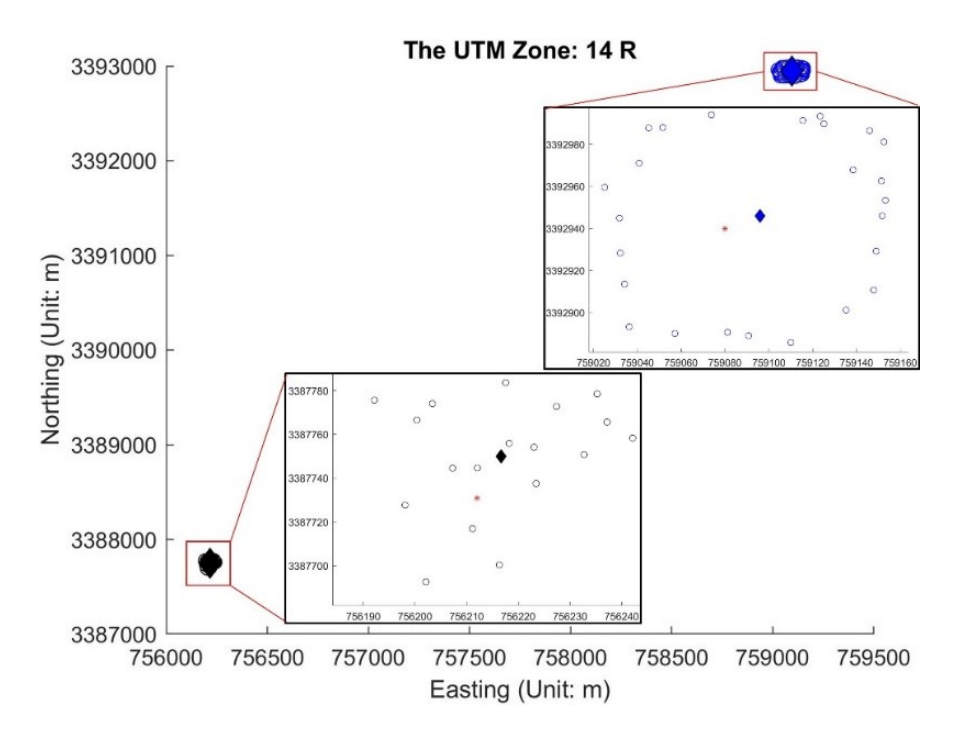


Fig. 7. An example of mean-shift clustering results (Circles: observers' locations, Diamonds: cluster centers, Bottom left cluster: fire hydrant #1, Upper right cluster: fire hydrant #2).

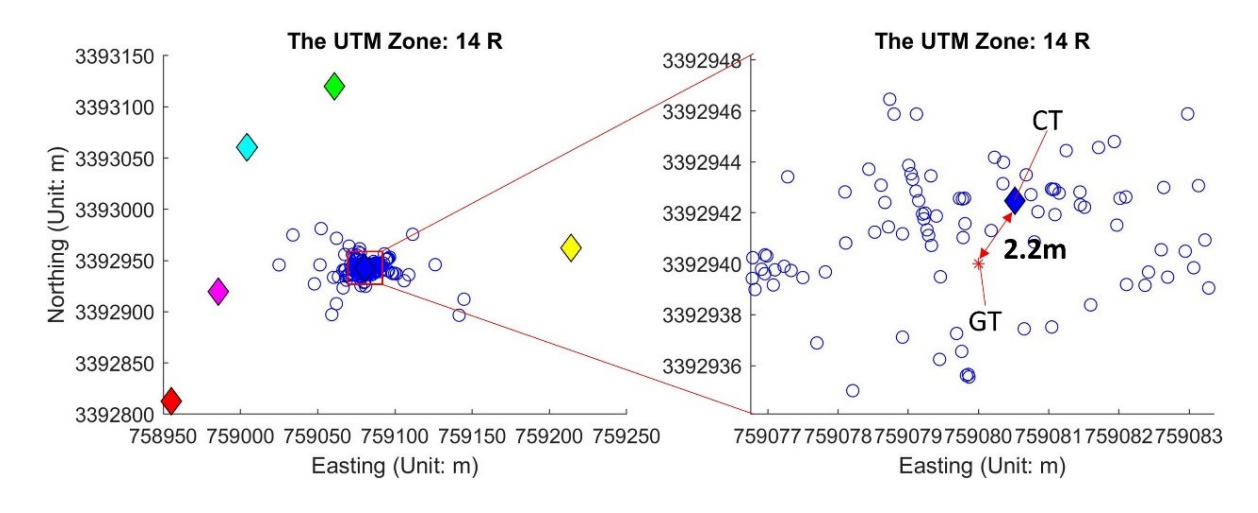


Fig. 8. Examples of the final estimated location (CT: a cluster center with the largest number of the estimated locations) and the ground truth (GT) of the fire hydrant #2 among the estimated locations (Circles).

Table 6. Examples of geospatial localization results in the case studies. The distance error values were obtained by averaging the geospatial localization results of 300 trials.

Target object	Number of data samples	Average distance from observers to a distant object	Distance error of the proposed method
Fire hydrant #1	18	34m	9.1m
Fire hydrant #2	25	62m	2.5m
Tower crane	22	186m	27.8m

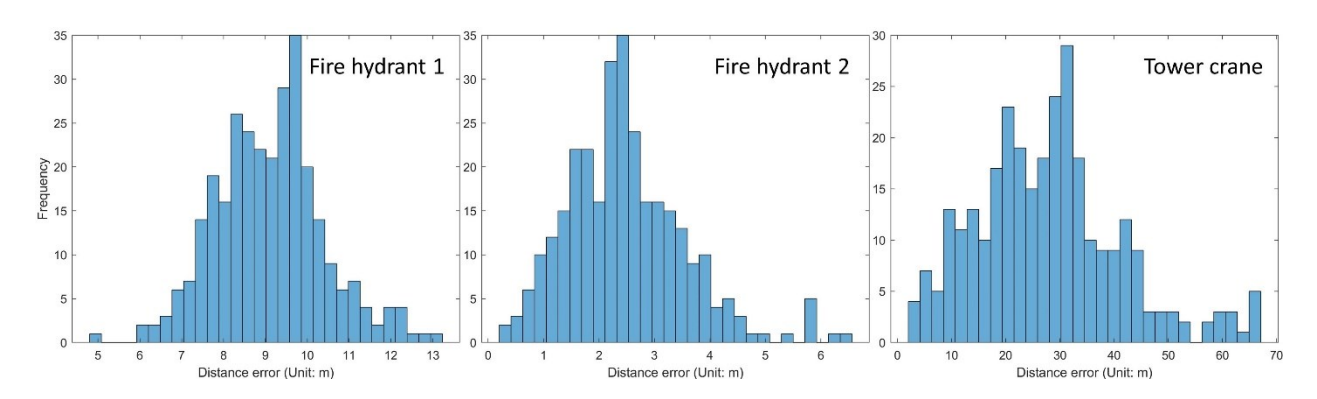


Fig. 9. Histograms regarding the distance error of the proposed method after 300 trials for each object.

To investigate the effect of the proximity between adjacent target objects, additional data samples were collected with respect to ten urban objects in Downtown Houston, as shown in Fig. 10. The proximity between these objects ranges from 128m to 261m. Sensitivity analysis was conducted to assess the effect of the window sizes of the mean-shift clustering at the preprocessing and postprocessing. The experimental results on the additional data set were shown in Fig. 11 and Table 7, obtained from averaging 300 localization experiments.



Fig. 10. The ground truth locations of ten urban objects (yellow pins) in Downtown Houston, TX. The enlarged regions display the data collection areas and the green dots represents the data sample locations.

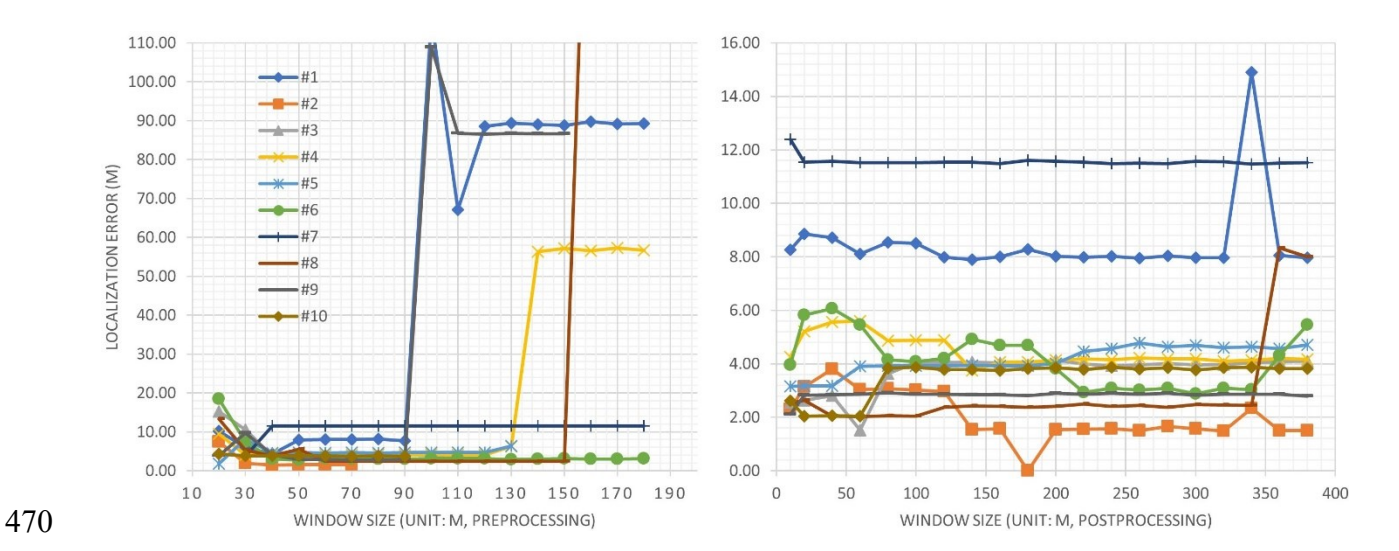


Fig. 11. Sensitivity Analysis for the window sizes of the mean-shift clustering at the preprocessing (Left) and the postprocessing (Right).

Table 7. Geospatial Localization results for ten objects in Downtown Houston, when the window sizes were 70m, and 300m for the preprocessing and postprocessing, respectively.

Distant Object	Obj.1	Obj.2	Obj.3	Obj.4	Obj.5	Obj.6	Obj.7	Obj.8	Obj.9	Obj.10
Photographer- to-object average distance (m)	38.1	26.8	31.3	20.0	22.8	28.0	23.8	38.7	24.5	22.2
Average distance error of a final estimated location (m)	8.0	1.5	4.0	4.3	4.7	3.0	11.5	2.4	2.8	3.8
Standard Deviation of Distance errors (m)	0.8	0.8	1.3	1.3	1.4	1.4	0.6	0.7	0.6	0.8
Average distance error of each estimated location (m)*	21.2	18.7	37.0	15.3	24.2	30.9	27.0	17.7	8.7	11.5

^{*}Before the postprocessing

5 Discussion

477

478

479

480

481

482

483

484

485

486

487

488

489

490

491

492

493

494

495

496

497

498

499

In the case study, the experiments demonstrated the effectiveness of the proposed method for localizing a distant object based on multiple observations. The recorded localization errors of 9.1m, 2.5m, and 27.8m for the target objects indicates that the proposed method has the potential to be used for localizing a distant object in participatory sensing, when citizens reports an event or an object of interest around them in urban areas. Table 8 shows that the errors of the proposed method were significantly lower than the average distance error of the estimated locations. The main reason for such performance improvement was attributed to the proposed mean-shift clustering module to determine the final location for a distant object among hundreds of the estimated locations obtained just by solving a system of line equations toward a distant object. In our case study, it was observed that distance errors of each estimated location (as shown as circles in Fig. 8) varied to a large extent. With the proposed mean-shift clustering module, the localization accuracy was able to be improved, and it was observed that the value of accuracy improvement is high when there are a lot of noisy data (i.e., outliers) in the dataset for the target object. As such, it is likely to yield a significant localization error of an estimated location at which the proposed mean-shift clustering module is not applied. Moreover, it was observed that the postprocessing module yielded relatively better and consistent localization results, even when noisy data was included in the localization process, as shown in Table 8. In the context of participatory sensing, such accuracy improvement is noteworthy since the reliability of crowdsourced data has been considered as one of the top challenges [54]. The performance improvement in localization might be explained using the central limit theorem of probability theory. The central limit theorem refers to the convergence of probability distributions of one or more random variables to a normal distribution, when the number of random variables increases [55]. In this context, an estimated

location of an object of interest can be regarded as a random variable of a normal distribution in which its parameter μ (mean) represents the ground truth location of the urban object. Thus, by determining the center of a cluster having the largest number of the estimated locations as the final location of an urban object, it was observed that the localization accuracy can be considerably improved in the case study. When the number of crowdsourced data is sufficient, it was observed that a similar localization accuracy was able to be obtained by using 10 or more line equations without the postprocessing module, as shown in Table 9. However, to obtain the best localization accuracy, it is recommended to use the postprocessing module since it can reduce the impact of noisy data, as shown in Table 9; the object detection model, R-FCN, should filter out noisy data to improve the localization accuracy in the preprocessing step. If the number of false positives is increased due to low performance of object detectors, the chance of involving noisy data in the process of the geospatial localization will be increased. Similarly, if the number of false negatives is increased due to the object detection failures (i.e., lack of the object detection model's performance), the correct data samples will not likely be included in the process of the geospatial localization. Therefore, the lack of the object detector's performance would lead to the escalation of localization error. It was observed that localization accuracy was deteriorated when noisy data were included, or the number of data samples was small, as presented in Table 8 and Table 10. Regarding the impact of the number of data samples, it was observed that the localization accuracy was relatively high and tended to converge when the number of data samples increased, as shown in Table 10 and Table 11.

520

521522

523

500

501

502

503

504

505

506

507

508

509

510

511

512

513

514

515

516

517

518

Table 8. Geospatial localization results for fire hydrant #2 when different numbers of noisy data were added to the original 25 data samples. (a-Number of noisy data, b-Distance error of the proposed method (m), c-Average distance error of each estimated locations (m))

a	21	20	19	18	17	16	15	14	13	12	11	10	9	8	7	6	5	4	3	2	1
b	9.6	8.2	8.2	7.4	7.0	7.0	6.9	6.2	5.7	5.9	5.7	5.7	4.8	4.5	3.6	3.5	3.4	2.6	1.8	1.8	2.7
c	124.6	123.1	126.1	120.3	124.3	126.9	119.4	122.1	92.9	92.4	91.3	88.1	93.3	95.0	93.5	101.3	37.5	30.6	26.5	22.4	18.6

Table 9. Geospatial localization results for fire hydrant #2 using different numbers of lines to estimate a final location. (**Group A-25** data samples, **Group B-25** data samples plus 21 noisy data samples, **a-**Distance error of the proposed method (m), **b-**Average distance error of each estimated locations (m), **c-**Number of lines used for localization)

	c	2	3	4	5	6	7	8	9	10	11	12	13	14	15	16	17	18	19	20
V dr	a	2.7	2.4	2.3	2.4	2.5	2.6	2.8	2.9	3.0	3.0	3.1	3.2	3.2	3.2	3.3	3.3	3.3	3.3	3.3
Group	b	12.5	6.4	5.5	5.0	4.6	4.4	4.2	4.0	3.9	3.8	3.7	3.6	3.5	3.5	3.5	3.4	3.4	3.4	3.4
B dr	a	9.5	16.8	18.1	18.5	19.1	19.7	20.5	21.2	21.7	22.1	22.5	22.7	22.9	23.0	23.1	23.2	23.3	23.4	23.5
Group B	b	118.0	33.9	28.9	27.1	26.3	25.6	25.2	24.9	24.7	24.5	24.4	24.3	24.2	24.2	24.1	24.1	24.1	24.1	24.1

Table 10. Sensitivity analysis for urban objects when the number of data samples, **c**, varies. (**a**-Distance error of the proposed method (m), **b**-Average distance error of each estimated locations (m), **c**-Number of data samples used in geospatial localization)

c	Fi hydra		hyd	ire Irant #2	Tower Crane			
	a	b	a	b	a	b		
3	8.9	9.8	2.9	4.1	47.8	120.0		
4	5.5	12.6	9.0	12.9	13.3	158.8		
5	7.6	12.5	6.2	17.7	23.9	120.7		
6	14.1	23.5	3.9	9.8	15.2	219908.0		
7	12.4	16.2	0.8	16.8	59.3	212.1		
8	11.2	17.9	1.6	9.8	32.1	262.0		
9	13.6	24.6	3.5	7.9	29.8	179.8		
10	10.2	17.7	3.9	14.9	43.2	8391.8		
11	11.1	22.8	3.5	10.0	35.1	204.3		
12	11.2	14.2	6.0	9.2	53.1	5765.5		
13	10.4	16.1	6.1	10.2	19.2	4934.1		
14	10.2	19.4	2.4	13.0	41.0	39598.8		
15	10.9	17.3	1.6 11.5		49.6	34563.0		
16	10.1	18.0	1.7	12.0	26.2	27962.0		
17	10.4	18.9	2.8	11.8	20.5	28273.3		

18	9.1	17.7	2.5	12.7	35.1	213.4
19	-	-	2.7	13.1	38.4	21216.8
20	-	-	3.0	13.7	37.8	17722.4
21	-	-	3.3	14.5	27.8	17341.6
22	-	-	2.2	12.0	-	-
23	-	-	2.3	13.0	-	-
24	-	-	2.6	12.8	-	-
25	-	-	2.7	12.5	-	-

Table 11. Sensitivity analysis of the number of data samples for ten objects in Downtown Houston. (a – The number of data samples)

	Distance error of the proposed method (m)											
a	Obj.1	Obj.2	Obj.3	Obj.4	Obj.5	Obj.6	Obj.7	Obj.8	Obj.9	Obj.10		
2	6.1	5.2	15.0	1.5	2.8	10.2	9.2	8.7	3.6	9.7		
3	7.0	11.1	9.8	5.4	13.3	11.6	3.0	11.4	3.7	5.2		
4	5.7	4.7	1.7	6.8	9.4	5.3	14.3	6.8	3.4	15.3		
5	11.2	4.4	7.8	4.0	3.8	18.2	10.6	10.4	1.7	7.5		
6	15.2	11.7	3.4	9.8	5.8	9.2	11.3	5.3	2.0	0.6		
7	11.6	2.0	2.9	8.0	3.6	2.1	9.3	2.7	2.8	3.8		
8	9.7	2.6	2.7	10.8	7.4	4.8	14.3	3.3	-	2.3		
9	8.8	0.6	7.0	5.9	1.6	5.9	11.5	3.8	-	3.8		
10	8.8	3.1	7.8	7.8	3.9	7.6	-	1.6	-	-		
11	8.9	5.1	7.0	3.9	-	3.5	-	2.4	-	-		
12	8.8	2.6	4.3	4.2	-	4.2	-	2.0	-	-		
13	10.9	3.9	5.6	5.1	-	-	-	-	-	-		
14	9.2	3.1	4.8	4.9	-	-	-	-	-	-		
15	9.2	4.2	3.6	-	-	-	-	-	-	-		
16	9.0	3.0	3.2	-	-	-	-	-	-	-		
17	8.2	-	4.4	-	-	-	-	-	-	-		
18	9.5	-	3.6	-	-	-	-	-	-	-		
19	8.9	-	-	-	-	-	-	-	-	-		
20	8.5	-	-	-	-	-	-	-	-	-		

The experimental results of the ten objects in Downtown Houston, presented in Table 7 and Fig. 10, showed that the proposed method is sensitive to the proximity between target objects. It was observed that when the window size of the mean-shift clustering at the preprocessing step was not properly selected, the localization error increased; when the window size was too large, the final locations could not be estimated due to the wrong selection of data samples, as observed in the left

graph in Fig. 11. It was observed that the window size at the postprocessing did not significantly affect the localization accuracy when the size was more than 60m. These results imply that the wrong selection of data samples for localization could result in a significant localization error or localization failure. Thus, the window size at the preprocessing step needs to be carefully determined.

542

543

544

545

546

547

548

549

550

551

552

553

554

555

556

557

558

559

560

561

562

563

564

To determine that the performance of the proposed method is good enough for the possible application, there is a need to define how much accuracy needs to be satisfied. However, to the best of the authors' knowledge, it is not trivial to determine the tolerable error ranges for localization that can be universally applied for the possible application. Rather, we compared the proposed method with prior works on finding the geographic location of distant objects only using embedded sensors in smartphone for the possible application. The required level of localization accuracy would vary depending on the purpose of application. In this context, we have selected the prior works that have the same/similar purpose with the proposed work. There have been prior studies dedicated to geospatial localization for distant objects or events using smartphones [11-13]. The localization method proposed by Manweiler et al. [11] has reported the distance errors ranging from 5m to 150m when the photographing distances to objects of interest ranged from 28m to 160m. Chen et al. [12] has reported the experimental results of their localization method comparing with the outcomes of Ouyang et al. (2013). The former reported the distanced errors from 8m to 35m when the distances to objects of interest were from 2m to 50m, while the latter recorded the distance error from 9m to 37m in the same experimental conditions. In this context, the experimental results of this case study indicate that the proposed method produces a reasonable localization accuracy, recording the distance errors of 1.5m to 27.8m (6.6m on average) when the distances to the objects of interest were 17m to 296m. The standard deviations of the distance errors, as shown in Table 7, shows the reliability of the localization results. Given the application of the proposed geospatial localization in this paper (i.e., enhanced disaster preparedness in urban built environments), the localization errors from the case studies seem to be acceptable for identifying distant objects at risk (when considering human range of sight). Based on the reported locations, site inspectors will be able to focus on selective areas for site inspection in order to facilitate disaster preparedness. Ultimately, in the author's opinions, the accuracy of the proposed method is expected to contribute to rapid data collection over large urban areas, thereby facilitating disaster preparedness that needs to identify locations of distant objects at risk.

The proposed localization method shows a potential of participatory sensing for various applications that needs to identify the locations of interest. For example, although municipal agencies manage public infrastructure assets based on GIS, conventional data collection such as site inspection with limited manpower may be suboptimal for monitoring numerous existing infrastructure assets in order to update the GIS within a short period time. Another example is that when an extreme weather event such as a hurricane is forecasted to come to a certain area, it is hard to inspect potentially vulnerable objects with limited manpower over large areas before the extreme weather strikes. In this respect, accurate location information from participatory sensing has a potential to facilitate disaster preparedness, because it allows municipal agencies to focus on selective locations for site inspection. A participatory sensing-based localization method for a distant object can be used in various applications, not limited to disaster preparedness.

6 Conclusion

Increasing occurrence of natural disasters has necessitated changes in conventional data collection

practices for preparedness, especially for urban areas where populations and vulnerable assets are concentrated. In this regard, this study was undertaken to devise a novel geospatial localization method that can be used to report distant objects vulnerable to extreme weather events for disaster preparedness. Building on the sequential computational algorithms in the proposed geospatial localization method —geographic coordinate conversion, the mean-shift clustering, deep learningbased object detection, magnetic declination adjustment, line of sight equation formulation, and the Moore-Penrose generalized inverse method—, distant objects in urban areas were able to be robustly localized with a reasonable accuracy. The experimental results show the potential of the proposed method in the context of participatory sensing, where the reliability of collected data varies to a great extent. The proposed method can be coupled with existing applications such as Google Street View or Google Map, and they would be a good avenue for visualizing the localization result by the proposed method. One of the significant findings to emerge from this study is that multiple observations from non-experts can be used to improve the geospatial localization accuracy, even when many noisy data are included. This finding has important implications for the understanding of how crowdsourced data should be processed to better understand local information in extensive urban areas. By leveraging the location information of local vulnerabilities to extreme weather events, practitioners can better understand where the focus is needed to reduce potential damage induced by severe weather in urban areas. One of the limitations lies in the preprocessing step. Still, there is a possibility that noisy data are included in the data cluster selected at the preprocessing step. An approach to tackle this issue could be to develop a robust filtering module to exclude noisy data that lack the accuracy of measured values such as compass bearings or geographic coordinates. The scope of this paper is the geospatial localization of distant (static) objects before extreme weather events in the context of disaster

587

588

589

590

591

592

593

594

595

596

597

598

599

600

601

602

603

604

605

606

607

608

preparedness, not damaged areas or moving objects during the events. To determine areas of interest, the proposed localization process might be applied to localize the areas. However, in this case, localization accuracy would be degraded due to inconsistent compass bearing because it is hard to determine a single point of interest representing the areas where a compass bearing should be measured. Thus, there is a need for more studies to robustly leverage the proposed geospatial localization to be used for localizing distant areas. In addition, there is a need for leveraging other sources of information (e.g., Google Street view that match collected photos involving target objects) to infer the direction information toward the target objects, which helps reduce participants' burden for reporting the direction information during the data collection. These are currently being explored as part of our ongoing research.

Acknowledgment

This material is in part based upon work supported by the National Science Foundation (NSF) under CMMI Award#1832187. In addition, this work was supported by the Department of Civil and Environmental Engineering and Engineering Mechanics at the University of Dayton. Any opinions, findings, and conclusions or recommendations expressed in this material are those of the author(s) and do not necessarily reflect the views of the funding agencies.

627 References

- J. Goldman, K. Shilton, J. Burke, D. Estrin, M. Hansen, N. Ramanathan, S. Reddy, V. Samanta, M. Srivastava, R. West, Participatory sensing: A citizen-powered approach to illuminating the patterns that shape our world, Foresight & Governance Project, White Paper (2009) 1-15, DOI, https://www.wilsoncenter.org/publication/participatory-sensing-citizen-powered-approach-to-illuminating-the-patterns-shape-our.
- D. Christin, A. Reinhardt, S.S. Kanhere, M. Hollick, A survey on privacy in mobile participatory sensing applications, Journal of Systems and Software 84 (11) (2011) 1928-1946, DOI: https://doi.org/10.1016/j.jss.2011.06.073.
- H.J. Henriksen, M.J. Roberts, P. van der Keur, A. Harjanne, D. Egilson, L. Alfonso, Participatory early warning and monitoring systems: A nordic framework for web-based flood risk management, International Journal of Disaster Risk Reduction (2018), DOI: https://doi.org/10.1016/j.ijdrr.2018.01.038.
- D. Alexander, Disaster and emergency planning for preparedness, response, and recovery, Oxford University Press, 2015 https://doi.org/10.1093/acrefore/9780199389407.013.12.
- F.H. Norris, S.P. Stevens, B. Pfefferbaum, K.F. Wyche, R.L. Pfefferbaum, Community resilience as a metaphor, theory, set of capacities, and strategy for disaster readiness, American Journal of Community Psychology 41 (1-2) (2008) 127-150, DOI: https://doi.org/10.1007/s10464-007-9156-6.
- 646 [6] R.-Q. Wang, H. Mao, Y. Wang, C. Rae, W. Shaw, Hyper-resolution monitoring of urban 647 flooding with social media and crowdsourcing data, Computers & Geosciences 111 (2018) 648 139-147, DOI: https://doi.org/10.1016/j.cageo.2017.11.008.
- C. Restrepo-Estrada, S.C. de Andrade, N. Abe, M.C. Fava, E.M. Mendiondo, J.P. de Albuquerque, Geo-social media as a proxy for hydrometeorological data for streamflow estimation and to improve flood monitoring, Computers & Geosciences 111 (2018) 148-158, DOI: https://doi.org/10.1016/j.cageo.2017.10.010.
- 653 [8] S.-W. Lo, J.-H. Wu, F.-P. Lin, C.-H. Hsu, Visual sensing for urban flood monitoring, Sensors 15 (8) (2015) 20006-20029, DOI: https://doi.org/10.3390/s150820006.
- Y. Ham, H. Yoon, Motion and visual data-driven distant object localization for field reporting, Journal of Computing in Civil Engineering 32 (4) (2018) 04018020, DOI: https://doi.org/10.1061/(ASCE)CP.1943-5487.0000767.
- K. Kim, H. Kim, Image-based construction hazard avoidance system using augmented reality in wearable device, Automation in Construction 83 (2017) 390-403,
 DOI: https://doi.org/10.1016/j.autcon.2017.06.014.
- J.G. Manweiler, P. Jain, R.R. Choudhury, Satellites in our pockets: An object positioning system using smartphones, Proceedings of the 10th international conference on Mobile

- systems, applications, and services, ACM, Low Wood Bay, Lake District, UK, 2012, pp. 211-224, DOI: https://doi.org/10.1145/2307636.2307656.
- H. Chen, B. Guo, Z. Yu, Q. Han, Toward real-time and cooperative mobile visual sensing and sharing, IEEE INFOCOM 2016 The 35th Annual IEEE International Conference on Computer Communications, 2016, pp. 1-9, DOI: https://doi.org/10.1109/INFOCOM.2016.7524481.
- R.W. Ouyang, A. Srivastava, P. Prabahar, R.R. Choudhury, M. Addicott, F.J. McClernon, If you see something, swipe towards it: Crowdsourced event localization using smartphones, Proceedings of the 2013 ACM international joint conference on Pervasive and ubiquitous computing, ACM, Zurich, Switzerland, 2013, pp. 23-32, DOI: https://doi.org/10.1145/2493432.2493455.
- [14] I. Ha, H. Kim, S. Park, H. Kim, Image retrieval using bim and features from pretrained vgg
 network for indoor localization, Building and Environment 140 (2018) 23-31, DOI:
 https://doi.org/10.1016/j.buildenv.2018.05.026.
- 677 [15] S.S. Kanhere, Participatory sensing: Crowdsourcing data from mobile smartphones in urban spaces, 2011 IEEE 12th International Conference on Mobile Data Management, Vol. 2, 2011, pp. 3-6, DOI: https://doi.org/10.1109/MDM.2011.16.
- 680 [16] M.D. Hendricks, M.A. Meyer, N.G. Gharaibeh, S. Van Zandt, J. Masterson, J.T. Cooper, J.A. Horney, P. Berke, The development of a participatory assessment technique for 681 infrastructure: Neighborhood-level monitoring towards sustainable infrastructure systems, 682 683 Sustainable Cities and Society 38 (2018)265-274, DOI: https://doi.org/10.1016/j.scs.2017.12.039. 684
- K. Chen, W. Lu, F. Xue, P. Tang, L.H. Li, Automatic building information model reconstruction in high-density urban areas: Augmenting multi-source data with architectural knowledge, Automation in Construction 93 (2018) 22-34, DOI: https://doi.org/10.1016/j.autcon.2018.05.009.
- 689 [18] Z. Zhou, J. Gong, X. Hu, Community-scale multi-level post-hurricane damage assessment 690 of residential buildings using multi-temporal airborne lidar data, Automation in 691 Construction 98 (2019) 30-45, DOI: https://doi.org/10.1016/j.autcon.2018.10.018.
- 692 [19] C.M. Yeum, A. Lund, S.J. Dyke, J. Ramirez, Automated recovery of structural drawing 693 images collected from postdisaster reconnaissance, Journal of Computing in Civil 694 Engineering 33 (1) (2019) 04018056, DOI: https://doi.org/10.1061/(ASCE)CP.1943-5487.0000798.
- Z. Zhou, J. Gong, M. Guo, Image-based 3d reconstruction for posthurricane residential
 building damage assessment, Journal of Computing in Civil Engineering 30 (2) (2016)
 04015015, DOI: https://doi.org/10.1061/(ASCE)CP.1943-5487.0000480.

- 699 [21] M.Z. Naser, V.K.R. Kodur, Cognitive infrastructure a modern concept for resilient 700 performance under extreme events, Automation in Construction 90 (2018) 253-264, DOI: 701 https://doi.org/10.1016/j.autcon.2018.03.004.
- [22] 702 F. Pena-Mora, J.K. Thomas, M. Golparvar-Fard, Z. Aziz, Supporting civil engineers during 703 disaster response and recovery using a segway mobile workstation chariot, Journal of Engineering 704 Computing in Civil 26 (2012)448-455, DOI: 705 https://doi.org/10.1061/(asce)cp.1943-5487.0000117.
- A.Y. Chen, F. Peña-Mora, A.P. Plans, S.J. Mehta, Z. Aziz, Supporting urban search and rescue with digital assessments of structures and requests of response resources, Advanced Engineering Informatics 26 (4) (2012) 833-845, DOI: https://doi.org/10.1016/j.aei.2012.06.004.
- 710 [24] A.Y. Chen, F. Pena-Mora, Y.F. Ouyang, A collaborative gis framework to support equipment distribution for civil engineering disaster response operations, Automation in Construction 20 (5) (2011) 637-648, DOI: https://doi.org/10.1016/j.autcon.2010.12.007.
- 713 [25] F. Pena-Mora, A.Y. Chen, Z. Aziz, L. Soibelman, L.Y. Liu, K. El-Rayes, C.A. Arboleda, T.S. Lantz, A.P. Plans, S. Lakhera, S. Mathur, Mobile ad hoc network-enabled collaboration framework supporting civil engineering emergency response operations, Journal of Computing in Civil Engineering 24 (3) (2010) 302-312, DOI: https://doi.org/10.1061/(asce)cp.1943-5487.0000033.
- 718 [26] J. Lee, Y. Jeong, Y.-S. Oh, J.-C. Lee, N. Ahn, J. Lee, S.-H. Yoon, An integrated approach 719 to intelligent urban facilities management for real-time emergency response, Automation 720 in Construction 30 (2013) 256-264, DOI: https://doi.org/10.1016/j.autcon.2012.11.008.
- 721 [27] S. Li, H. Cai, V.R. Kamat, Uncertainty-aware geospatial system for mapping and visualizing underground utilities, Automation in Construction 53 (2015) 105-119, DOI: https://doi.org/10.1016/j.autcon.2015.03.011.
- 724 [28] H. Yoon, R. Shiftehfar, S. Cho, B.F. Spencer, M.E. Nelson, G. Agha, Victim localization 725 and assessment system for emergency responders, Journal of Computing in Civil 726 Engineering 30 (2) (2016) 04015011, DOI: https://doi.org/10.1061/(ASCE)CP.1943-5487.0000483.
- 728 [29] M.M. Torok, M. Golparvar-Fard, K.B. Kochersberger, Image-based automated 3d crack 729 detection for post-disaster building assessment, Journal of Computing in Civil Engineering 730 28 (5) (2014) A4014004, DOI: https://doi.org/10.1061/(ASCE)CP.1943-5487.0000334.
- 731 [30] C. Koch, K. Georgieva, V. Kasireddy, B. Akinci, P. Fieguth, A review on computer vision 732 based defect detection and condition assessment of concrete and asphalt civil infrastructure, 733 Advanced Engineering Informatics 29 (2015)196-210, DOI: (2) http://dx.doi.org/10.1016/j.aei.2015.01.008. 734

- V. Balali, A. Jahangiri, S.G. Machiani, Multi-class us traffic signs 3d recognition and localization via image-based point cloud model using color candidate extraction and texture-based recognition, Advanced Engineering Informatics 32 (2017) 263-274, DOI: https://doi.org/10.1016/j.aei.2017.03.006.
- 739 [32] Y. Wei, V. Kasireddy, B. Akinci, 3d imaging in construction and infrastructure management: Technological assessment and future research directions, Workshop of the European Group for Intelligent Computing in Engineering, Springer, 2018, pp. 37-60, DOI: https://doi.org/10.1007/978-3-319-91635-4 3.
- E.B. Anil, B. Akinci, J.H. Garrett, O. Kurc, Characterization of laser scanners for detecting cracks for post-earthquake damage inspection, Proceedings of the International Symposium on Automation and Robotics in Construction, 2013, pp. 313-320, DOI: https://doi.org/10.22260/ISARC2013/0034.
- 747 [34] M. Choi, R. Starbuck, S. Lee, S. Hwang, S. Lee, M. Park, H.-S. Lee, Distributed and interoperable simulation for comprehensive disaster response management in facilities, Automation in Construction 93 (2018) 12-21, DOI: https://doi.org/10.1016/j.autcon.2018.05.007.
- 751 [35] G. Bunea, F. Leon, G.M. Atanasiu, Postdisaster evacuation scenarios using multiagent system, Journal of Computing in Civil Engineering 30 (6) (2016) 05016002, DOI: https://doi.org/10.1061/(ASCE)CP.1943-5487.0000575.
- 754 [36] C. Xiong, X. Lu, M. Hori, H. Guan, Z. Xu, Building seismic response and visualization using 3d urban polygonal modeling, Automation in Construction 55 (2015) 25-34, DOI: https://doi.org/10.1016/j.autcon.2015.03.023.
- 757 [37] S.-Y. Lin, W.-C. Chuang, L. Xu, S. El-Tawil, S.M.J. Spence, V.R. Kamat, C.C. Menassa, J. McCormick, Framework for modeling interdependent effects in natural disasters: Application to wind engineering, Journal of Structural Engineering 145 (5) (2019) 04019025, DOI: https://doi.org/10.1061/(ASCE)ST.1943-541X.0002310.
- 761 [38] M. Pelling, Learning from others: The scope and challenges for participatory disaster risk assessment, Disasters 31 (4) (2007) 373-385, DOI: https://doi.org/10.1111/j.1467-7717.2007.01014.x.
- 764 [39] W. Liu, S. Dugar, I. McCallum, G. Thapa, L. See, P. Khadka, N. Budhathoki, S. Brown, R. Mechler, S. Fritz, P. Shakya, Integrated participatory and collaborative risk mapping for enhancing disaster resilience, ISPRS International Journal of Geo-Information 7 (2) (2018) 68, DOI: https://doi.org/10.3390/ijgi7020068.
- 768 [40] Q. Huang, Y. Xiao, Geographic situational awareness: Mining tweets for disaster 769 preparedness, emergency response, impact, and recovery, ISPRS International Journal of Geo-Information 4 (3) (2015) 1549, DOI: https://doi.org/10.3390/ijgi4031549.

- J.P. De Albuquerque, B. Herfort, A. Brenning, A. Zipf, A geographic approach for combining social media and authoritative data towards identifying useful information for disaster management, International Journal of Geographical Information Science 29 (4) (2015) 667-689, DOI: https://doi.org/10.1080/13658816.2014.996567.
- 775 [42] D. Eilander, P. Trambauer, J. Wagemaker, A. van Loenen, Harvesting social media for generation of near real-time flood maps, Procedia Engineering 154 (2016) 176-183, DOI: https://doi.org/10.1016/j.proeng.2016.07.441.
- 778 [43] J. Fohringer, D. Dransch, H. Kreibich, K. Schröter, Social media as an information source 779 for rapid flood inundation mapping, Natural Hazards and Earth System Sciences 15 (12) 780 (2015) 2725-2738, DOI: https://doi.org/10.5194/nhess-15-2725-2015.
- 781 [44] W.-Y. Lin, T.-H. Wu, M.-H. Tsai, W.-C. Hsu, Y.-T. Chou, S.-C. Kang, Filtering disaster responses using crowdsourcing, Automation in Construction 91 (2018) 182-192, DOI: https://doi.org/10.1016/j.autcon.2018.03.016.
- 784 [45] A.A. Marquez, P. Venturino, J.L. Otegui, Common root causes in recent failures of cranes,
 785 Engineering Failure Analysis 39 (2014) 55-64, DOI:
 786 https://doi.org/10.1016/j.engfailanal.2014.01.012.
- 787 [46] N. Piasco, D. Sidibé, C. Demonceaux, V. Gouet-Brunet, A survey on visual-based localization: On the benefit of heterogeneous data, Pattern Recognition 74 (2018) 90-109, DOI: https://doi.org/10.1016/j.patcog.2017.09.013.
- 790 [47] D. Wang, L. Kaplan, H. Le, T. Abdelzaher, On truth discovery in social sensing: A maximum likelihood estimation approach, Proceedings of the 11th international conference on Information Processing in Sensor Networks, ACM, 2012, pp. 233-244, DOI: https://doi.org/10.1109/IPSN.2012.6920960.
- 794 [48] C. Yizong, Mean shift, mode seeking, and clustering, IEEE Transactions on Pattern 795 Analysis and Machine Intelligence 17 (8) (1995) 790-799, DOI: 796 https://doi.org/10.1109/34.400568.
- 797 J. Dai, Y. Li, K. He, J. Sun, R-fcn: Object detection via region-based fully convolutional [49] 798 Advances in neural information processing systems, Neural Information networks. 799 Processing Systems Foundation. 2016. 379-387, DOI. pp. 800 http://papers.nips.cc/paper/6465-r-fcn-object-detection-via-region-based-fully-801 convolutional-networks.
- 802 [50] Y. LeCun, Y. Bengio, G. Hinton, Deep learning, Nature 521 (7553) (2015) 436-444, DOI: http://dx.doi.org/10.1038/nature14539.
- N. National Centers for Environmental Information, Magnetic field calculators, Vol. Oct. 10, 2018, National Oceanic and Atmospheric Administration (NOAA), 2018, DOI, https://www.ngdc.noaa.gov/geomag-web/#declination.

D. Serre, Matrices: Theory and applications, 2nd ed., Springer, New York, USA, 2010 807 [52] 808 https://doi.org/10.1007/978-1-4419-7683-3 ISBN: 978-1-4419-7682-6. 809 [53] S. Ren, K. He, R. Girshick, J. Sun, Faster r-cnn: Towards real-time object detection with 810 region proposal networks, Advances in neural information processing systems, Neural 811 Information Processing Systems Foundation, 91-99, 2015, http://papers.nips.cc/paper/5638-faster-r-cnn-towards-real-time-object-detection-with-812 813 region-proposal-networks. 814 R.I. Ogie, H. Forehead, R.J. Clarke, P. Perez, Participation patterns and reliability of [54] 815 human sensing in crowd-sourced disaster management, Information Systems Frontiers 20 816 (4) (2018) 713-728, DOI: https://doi.org/10.1007/s10796-017-9790-y. 817 H. Fischer, A history of the central limit theorem: From classical to modern probability [55] 818 theory, Springer Science & Business Media, New York, 10013, USA, 2010 https://doi.org/10.1007/978-0-387-87857-7 ISBN: 978-0-387-87856-0. 819 820

822 Appendix

The process of the geospatial localization

With the adjusted compass heading, a line equation toward a distant object of interest can be formulated as follows:

$$y = \tan(90^\circ - \theta - \varepsilon) \cdot (x - x_1) + y_1 \tag{1}$$

where x: Easting, y: Northing, θ : compass bearing, ε : magnetic declination, x_1 : the Easting of a data sample, and y_1 : the Northing of a data sample.

828

829

830

831

832

By equation (1), every data sample has its own line equation with respect to a distant object of interest. In principle, the estimated location of a distant object can be obtained by solving multiple line equations, even if the number of line equations is greater than the number of unknowns (x, y)—Easting and Northing. To obtain a unique solution, multiple line equations are computed as a linear combination as follows:

834

833

$$x \begin{bmatrix} a_{11} \\ a_{21} \\ \vdots \\ a_{n1} \end{bmatrix} + y \begin{bmatrix} a_{12} \\ a_{22} \\ \vdots \\ a_{n2} \end{bmatrix} = \begin{bmatrix} b_1 \\ b_2 \\ \vdots \\ b_n \end{bmatrix}$$
 (2)

where x: Easting, y: Northing, a_{n1} is a coefficient of x, a_{n2} is a coefficient of y, and b_n is a constant.

Equation (2) can be represented as a system of linear equations, as follows:

$$AL = b (3)$$

where $A = \begin{bmatrix} a_{11} & a_{12} \\ a_{21} & a_{22} \\ \vdots & \vdots \\ a_{n1} & a_{n2} \end{bmatrix}$, $L = \begin{bmatrix} x \\ y \end{bmatrix}$, $b = \begin{bmatrix} b_1 \\ b_2 \\ \vdots \\ b \end{bmatrix}$, a_{n1} is a coefficient of x, a_{n2} is a coefficient of y, 838

and b_n is a constant 839

840

841

The estimated location of L can be derived by solving equation (3). When n > 2, the matrix A becomes singular and thus is not invertible. In such cases, a pseudoinverse matrix A⁺ derived by 842 843 the Moore-Penrose generalized inverse [52] is used to obtain a unique solution for equation (3), as follows: 844

845

$$A^{+}AL = A^{+}b \tag{4}$$

$$L = A^+b \tag{5}$$

where A^+ satisfies the four properties of (1) $AA^+A=A$, (2) $A^+AA^+=A^+$, (3) $(AA^+)^T=AA^+$, and 846 (4) $(A^+A)^T = A^+A$, when the elements of A are real numbers. By equation (5), the location of a distant object can be estimated building upon multiple line equations, if the number of line 848 849 equations is 2 or above.

850